2D gravity inversion with isostatic constraint applied to passive rifted margins

B. Marcela S. Bastos[*] and Vanderlei C. Oliveira Jr[*]

[*]*Observatório Nacional,*

Department of Geophysics,

Rio de Janeiro, Brazil

(August 28, 2018)

GEO-XXXX

Running head: **2D gravity inversion for passive rifted margins**

ABSTRACT

Lorem ipsum dolor sit amet, consectetuer adipiscing elit. Ut purus elit, vestibulum ut, placerat ac, adipiscing vitae, felis. Curabitur dictum gravida mauris. Nam arcu libero, nonummy eget, consectetuer id, vulputate a, magna. Donec vehicula augue eu neque. Pellentesque habitant morbi tristique senectus et netus et malesuada fames ac turpis egestas. Mauris ut leo. Cras viverra metus rhoncus sem. Nulla et lectus vestibulum urna fringilla ultrices. Phasellus eu tellus sit amet tortor gravida placerat. Integer sapien est, iaculis in, pretium quis, viverra ac, nunc. Praesent eget sem vel leo ultrices bibendum. Aenean faucibus. Morbi dolor nulla, malesuada eu, pulvinar at, mollis ac, nulla. Curabitur auctor semper nulla. Donec varius orci eget risus. Duis nibh mi, congue eu, accumsan eleifend, sagittis quis, diam. Duis eget orci sit amet orci dignissim rutrum.

INTRODUCTION

Several methods have been proposed for using gravity and/or magnetic data to estimate the boundaries of adjacent sedimentary layers, the relief of basement under sedimentary basins and/or the Mohorovicic discontinuity (or simply Moho), which separates crust and mantle. These geophysical discontinuities represent, for such particular methods, density and/or magnetization contrasts in subsurface. All these methods suffer from the inherent ambiguity (Roy, 1962; Skeels, 1947) in determining the true physical property distribution from a discrete set of observed potential-field data. It is well known that, by using different physical property values, it is possible to find different interfaces producing the same potential-field data. To partially overcome this problem and obtain meaningful solutions, the interpreter must commonly use priori information obtained from seismic data and/or boreholes in order to constrain the range of possible models.

There are methods that approximate the subsurface by a grid of juxtaposed cells with constant physical property. Then they estimate the physical property value of each cell and finally use the estimated values to estimate the geometry of the geophysical discontinuities. Notice that, in this case, the geometry of the geophysical discontinuities are estimated in an indirect way. Although very useful in geophysics, such methods are outside the scope of the present work. Here, we consider methods that represent discontinuities by interfaces separating layers with constant or depth-dependent physical property distribution (density and/or magnetization). In this case, the geometry of the geophysical discontinuities are directly determined by estimating the geometrical parameters describing the interfaces.

Different criteria can be used to classify these methods. Those applied over a sedimentary basin, for example, are considered local scale methods, whereas those applied over a

continent or country are considered regional scale methods and those applied over the whole globe are considered global scale methods. Examples of local scale methods estimating the geometry of a single interface separating two layers were presented by Bott (1960); Tanner (1967); Cordell and Henderson (1968); Dyrelius and Vogel (1972); Pedersen (1977); Pilkington and Crossley (1986a); Richardson and MacInnes (1989); Barbosa et al. (1997, 1999b,a); Silva et al. (2006); Pilkington (2006); Chakravarthi and Sundararajan (2007); Martins et al. (2010); Silva et al. (2010); Lima et al. (2011); Martins et al. (2011); Barnes and Barraud (2012); Silva et al. (2014); Silva and Santos (2017), in the space domain, and Oldenburg (1974); Granser (1987); Reamer and Ferguson (1989); Guspí (1993), in the Fourier domain. Most of these methods were applied to estimate the relief of basement under a sedimentary basin. Methods estimating a single interface representing the Moho, at regional scale, were presented by Shin et al. (2009); Bagherbandi and Eshagh (2012); Barzaghi and Biagi (2014); Sampietro (2015); Uieda and Barbosa (2017), in space domain, and by Braitenberg et al. (1997); Braitenberg and Zadro (1999); van der Meijde et al. (2013) in Fourier domain. There are also some global scale methods (e.g., Sünkel, 1985; Sjöberg, 2009).

The regional and global scale methods usually presume that the interface representing the Moho oscillates around a reference depth.

The regional and global scale methods usually presume that the crust and mantle are at isostatic equilibrium.

MULTILAYER METHODS

The second group of methods is formed by those estimating multiple interfaces separating layers with constant physical properties.

(Pilkington and Crossley, 1986b; Gallardo et al., 2005; Camacho et al., 2011; Salem

et al., 2014)

All these methods have been applied at local scale, to characterize a single sedimentary basin, for example.

The number of methods forming this group is significantly lower than that of the other one.

They suffer from a greater ambiguity if compared to those of the first group. Consequently, the methods forming the second group require more priori information to decrease the number of possible solutions.

Few methods using gravity data have imposed isostatic equilibrium to the estimated interface(s).

Most of them estimate a single interface representing the Moho (e.g., Bagherbandi and Eshagh, 2012; Sampietro, 2015; Sjöberg, 2009).

These methods are applied at regional and global scales.

Salem et al. (2014) presented one of the few methods that impose isostatic equilibrium to a set of two interfaces representing the basement and Moho geometries under a sedimentary basin, at local scale.

METHODOLOGY

Forward problem

Let $\mathbf{d}^o$ be the observed data vector, whose i-th element d_i^o, $i = 1, \ldots, N$, represent the observed gravity disturbance at the point (x_i, y_i, z_i), on a profile located over a rifted passive margin. The coordinates are referred to a topocentric Cartesian system, with z axis pointing

downward, y-axis along the profile and x-axis perpendicular to the profile. We assume that the actual mass distribution in a rifted passive margin can be schematically represented according to Figure 1. In this model, the subsurface is formed by four layers. The first and shallowest one represents a water layer with constant density $\rho^{(w)}$. The second layer is formed by Q vertically adjacent parts representing sediments, salt or volcanic rocks. In our example, this layer is formed by two parts with constant densities $\rho^{(q)}$, $q = 1, 2$. Different models can be created by changing Q. The third layer of our model represents the crust. For simplicity, we presume that the crust density may be equal to $\rho^{(cc)}$, which represents the continental crust, or equal to $\rho^{(oc)}$, which represents the oceanic crust. The deepest layer represents a homogeneous mantle with constant density $\rho^{(m)}$. The interface separating the second and third layers defines the basement relief whereas that separating the third and fourth layers defines the Moho (represented by dashed-white line in Figure 1). In order to define the anomalous mass distribution producing the observed gravity disturbance data, we presume a reference mass distribution formed by two homogeneous layers (not shown). The shallowest layer represents the crust, the deepest layer represents the mantle and the interface separating them is conveniently called reference Moho (represented as a continuous white line in Figure 1). The reference mass distribution can be thought of as the outer layers of a concentric mass distribution producing the normal gravity field. We also presume the existence of an isostatic compensation depth at S_0 (represented as a continuous white line in Figure 1).

We consider that the anomalous mass distribution producing the observed data is defined as the difference between the rifted margin model (Figure 1) and the reference mass distribution (not shown). This anomalous mass distribution is approximated by an interpretation model formed by N columns of vertically stacked prisms (Figure 2). For convenience,

we presume that there is an observed gravity disturbance ...

PAREI AQUI

We consider that the prisms in the extremities of the interpretation model extend to infinity along the y axis in order to prevent edge effects in the forward calculations. The i-th column is formed by four vertically adjacent layers, which in turn are composed of vertically adjacent prisms having infinite length along the x-axis.

The first and shallowest layer represents the water layer, is formed by a single prism, has thickness t_i^w and a constant density contrast $\Delta \rho^w = \rho^w - \rho^r$, where ρ^w and ρ^r represents, respectively, the densities of water and the reference mass distribution (Figure **??**) at the same point. The third layer represents the crust, it is also formed by a single prism, has thickness t_i^c and density contrast $\Delta \rho_i^c = \rho^c - \rho^r$, with ρ^c being the crust density. For simplicity, we presume that the crust density ρ_i^c may be equal to ρ^{cc}, for $y_i \leq y_{COT}$, which represents continental crust, or equal to ρ^{oc}, for $y_i > y_{COT}$, which represents oceanic crust. The crust density depends on the position of the i-th column with respect to y_{COT}, which defines an abrupt Crust-Ocean Transition (COT). Consequently, the crust may have two possible density contrasts: $\Delta \rho_i^c = \rho^{cc} - \rho r$ or $\Delta \rho_i^c = \rho^{oc} - \rho^r$. The top of this layer defines the basement relief and its bottom the relief of the Moho. The fourth layer represents the mantle, it is divided into two parts, each one formed by a single prism having the same density ρ^m and, consequently, the same density contrast $\Delta \rho^m = \rho^m - \rho^r$. The shallowest portion of this layer has thickness t_i^m. Its top and bottom define, respectively, the depths of Moho and the planar isostatic compensation layer S_0. The deepest portion of the fourth layer has thickness ΔS_0, top at the surface S_0 and bottom at the planar surface $S_0 + \Delta S_0$, which defines the Moho in the reference mass distribution model (Figure **??**).

Finally, the second layer forming the t-th column of the interpretation model is defined by the interpreter, according to the geological environment to be studied and the a priori information availability. As a general rule, this layer can be defined by a set of Q vertically adjacent prisms, each one with thickness t_i^q, density ρ^q and density contrast $\Delta\rho^q = \rho^q - \rho^r$, $q = 1, \ldots Q$.

Given the density contrasts, the COT position y_{COT}, the isostatic compensation surface S_0, the thickness of the water layer and of the $Q-1$ prisms forming the shallowest portion of the second layer, it is possible to describe the interpretation model in terms of an $M \times 1$ parameter vector $\mathbf{p}$, $M = 2N + 1$, defined as follows:

$$\mathbf{p} = \begin{bmatrix} \mathbf{t}^Q \\ \mathbf{t}^m \\ \Delta S_0 \end{bmatrix}, \tag{1}$$

where $\mathbf{t}^Q$ and $\mathbf{t}^m$ are $N \times 1$ vectors whose i-th elements t_i^Q and t_i^m represent, respectively, the thickness of the prism forming the deepest portion of the second layer and the thickness of the prism forming the shallowest portion of the fourth layer of the interpretation model. In this case, the gravity disturbance produced by the interpretation model (the predicted gravity disturbance) at the position (x_i, y_i, z_i) can be written as the sum of the vertical component of the gravitational attraction exerted by the L prisms forming the interpretation model as follows:

$$d_i(\mathbf{p}) = k_g\, G \sum_{j=1}^{L} f_{ij}(\mathbf{p}), \tag{2}$$

where $f_{ij}(\mathbf{p})$ represents an integral over the volume of the j-th prism. Here, these volume integrals are computed with the expressions proposed by Nagy et al. (2000), by using the open-source Python package *Fatiando a Terra* (Uieda et al., 2013).

Inverse problem

Let $\mathbf{d}(\mathbf{p})$ be the predicted data vector, whose i-th element $d_i(\mathbf{p})$ is defined by Equation 2. Estimating the particular parameter vector $\mathbf{p} = \hat{\mathbf{p}}$ producing a predicted data vector $\mathbf{d}(\mathbf{p})$ as close as possible to the observed data vector $\mathbf{d}^o$ can be formulated as the problem of minimizing the goal function

$$\Gamma(\mathbf{p}) = \Phi(\mathbf{p}) + \mu \sum_{k=0}^{3} \alpha_k \Psi_k(\mathbf{p}) \, , \tag{3}$$

subject to all elements of $\hat{\mathbf{p}}$ be positive. In Equation 3, μ represents the regularizing parameter, $\Phi(\mathbf{p})$ represents the misfit function given by

$$\Phi(\mathbf{p}) = \frac{1}{N} \|\mathbf{d}^o - \mathbf{d}(\mathbf{p})\|_2^2 \, , \tag{4}$$

where $\|\cdot\|_2^2$ represents the squared Euclidean norm, α_k represent the weights assigned to the regularizing functions $\Psi_k(\mathbf{p})$, with define the constraints on the parameters to be estimated, $k = 0, 1, 2, 3$.

Airy constraint

Consider that the interpretation model is in isostatic equilibrium according to the Airy model (Turcotte and Schubert, 2002; Hofmann-Wellenhof and Moritz, 2005; Lowrie, 2007). In this case, the pressure (or lithostatic stress) exerted by the model is constant on the isostatic compensation surface S_0. The pressure per unit area exerted by the i-th column of the model on S_0, divided by gravity, is given by:

$$t_i^w \rho^w + t_i^1 \rho_i^1 + \cdots + t_i^Q \rho_i^Q + t_i^c \rho_i^c + t_i^m \rho^m = \sigma_0 \, , \tag{5}$$

where σ_0 is an arbitrary positive constant. Rearranging terms in Equation 5 and using the relation

$$S_0 = t_i^w + t_i^1 + \cdots + t_i^Q + t_i^c + t_i^m \,, \tag{6}$$

it is possible to show that:

$$(\rho_i^Q - \rho_i^c)\, t_i^Q + (\rho^m - \rho_i^c)\, t_i^m + (\rho^w - \rho_i^c)\, t_i^w + (\rho_i^1 - \rho_i^c)\, t_i^1 + \cdots + (\rho_i^{Q-1} - \rho_i^c)\, t_i^{Q-1} + \rho_i^c\, S_0 = \sigma_0. \tag{7}$$

In order to describe the pressure exerted by all columns forming the interpretation model on the surface S_0, Equation 7 can be written, in matrix notation, as follows:

$$\mathbf{M}^Q \mathbf{t}^Q + \mathbf{M}^m \mathbf{t}^m + \mathbf{M}^w \mathbf{t}^w + \mathbf{M}^1 \mathbf{t}^1 + \cdots + \mathbf{M}^{Q-1} \mathbf{t}^{Q-1} + \boldsymbol{\rho}^c S_0 = \sigma_0 \mathbf{1} \,, \tag{8}$$

where $\mathbf{1}$ is an $N \times 1$ vector with all elements equal to one, $\mathbf{t}^\alpha$ are $N \times 1$ vectors with i-th element defined by the thickness t_i^α of a prism forming the i-th column, $\alpha = w, 1, \ldots, Q-1, Q, m$, and $\mathbf{M}^Q$, $\mathbf{M}^m$, $\mathbf{M}^w$, $\mathbf{M}^1$, $\ldots$, $\mathbf{M}^{Q-1}$ are $N \times N$ diagonal matrices with elements ii of main diagonal are given by density contrasts $(\rho_i^Q - \rho_i^c)$, $(\rho^m - \rho_i^c)$, $(\rho^w - \rho_i^c)$, $(\rho_i^1 - \rho_i^c)$ and $\ldots$, $(\rho_i^{Q-1} - \rho_i^c)$, respectively, and $\boldsymbol{\rho}^c$ is an $N \times 1$ vector containing the densities of the prisms representing the crust. By applying the first-order Tikhonov regularization (Aster et al., 2005) to the constant vector $\sigma_0 \mathbf{1}$, we obtain the following expression:

$$\mathbf{R}\,(\mathbf{C}\mathbf{p} + \mathbf{D}\mathbf{t}) = \mathbf{0} \,, \tag{9}$$

where $\mathbf{0}$ is a vector with null elements and the remaining terms are given by:

$$\mathbf{C} = \begin{bmatrix} \mathbf{M}^Q & \mathbf{M}^m & \mathbf{0} \end{bmatrix}_{N \times M} \,, \tag{10}$$

$$\mathbf{D} = \begin{bmatrix} \mathbf{M}^w & \mathbf{M}^1 & \cdots & \mathbf{M}^{Q-1} & \boldsymbol{\rho}^c \end{bmatrix}_{N \times (QN+1)} \,, \tag{11}$$

$$\mathbf{t} = \begin{bmatrix} \mathbf{t}^w \\ \mathbf{t}^1 \\ \vdots \\ \mathbf{t}^{Q-1} \\ S_0 \end{bmatrix}_{(QN+1)\times 1}, \tag{12}$$

$\mathbf{p}$ is the parameter vector (Equation 1) and $\mathbf{R}$ is an $(N-1) \times N$ matrix, whose element ij is defined as follows:

$$[\mathbf{R}]_{ij} = \begin{cases} 1 & , \quad j = i \\ -1 & , \quad j = i+1 \\ 0 & , \quad \text{otherwise} \end{cases} . \tag{13}$$

Finally, from Equation 9, it is possible to define the regularizing function $\Psi_0(\mathbf{p})$ (Equation 3):

$$\Psi_0(\mathbf{p}) = \|\mathbf{R} \left(\mathbf{C}\mathbf{p} + \mathbf{D}\mathbf{t}\right)\|_2^2 . \tag{14}$$

We call this function as *Airy constraint*. Notice that minimizing this function imposes smoothness on the pressure exerted by the interpretation model on the isostatic compensation surface S_0.

Smoothness constraint

This constraint imposes smoothness on the adjacent thickness of the prisms forming the deepest portion of the second layer and the shallowest part of the fourth layer of the interpretation model by applying the first-order Tikhonov regularization (Aster et al., 2005) to the vectors $\mathbf{t}^Q$ and $\mathbf{t}^m$ (Equation 1). Mathematically, this constraint is represented by the

regularizing function $\Psi_1(\mathbf{p})$ (Equation 3):

$$\Psi_1(\mathbf{p}) = \|\mathbf{Sp}\|_2^2, \tag{15}$$

where $\mathbf{S}$ is an $(N-1) \times M$ matrix given by:

$$\mathbf{S} = \begin{bmatrix} \mathbf{R} & \mathbf{R} & \mathbf{0} \end{bmatrix}, \tag{16}$$

where $\mathbf{R}$ is defined by Equation 13 and $\mathbf{0}$ is a vector with all elements equal to zero.

Equality constraint

Equality constraint on basement depths

Let $\mathbf{a}$ be a vector whose k-th element a_k, $k = 1, \ldots, A$, is the known basement depth at the horizontal coordinate y_k^A of the profile. These known basement depth values are used to define the regularizing function $\Psi_2(\mathbf{p})$ (Equation 3):

$$\Psi_2(\mathbf{p}) = \|\mathbf{Ap} - \mathbf{a}\|_2^2, \tag{17}$$

where $\mathbf{A}$ is an $A \times M$ matrix whose k-th line has one element equal to one and all the remaining elements equal to zero. The location of the single non-null element in the k-th line of $\mathbf{A}$ depends on the coordinate y_k^A of the known basement depth a_k. Let us consider, for example, an interpretation model formed by $N = 10$ columns. Consider also that the basement depth at the coordinates $y_1^A = y_4$ and $y_2^A = y_9$ of the profile are equal to 25 and 35.7 km, respectively. In this case, $A = 2$, $\mathbf{a}$ is a 2×1 vector with elements $a_1 = 25$ and $a_2 = 35.7$ and $\mathbf{A}$ is a $2 \times M$ matrix ($M = 2N + 1 = 21$). The element 4 of the first line and the element 9 of the second line of $\mathbf{A}$ are equal to 1 and all its remaining elements are equal to zero.

Let $\mathbf{b}$ be a vector whose k-th element b_k, $k = 1, \ldots, B$, is the difference between the isostatic compensation depth S_0 and the known Moho depth at the horizontal coordinate y_k^B of the profile. These differences, which must be positive, are used to define the regularizing function $\Psi_3(\mathbf{p})$ (Equation 3):

$$\Psi_3(\mathbf{p}) = \|\mathbf{B}\mathbf{p} - \mathbf{b}\|_2^2 \,, \tag{18}$$

where $\mathbf{B}$ is a $B \times M$ matrix whose k-th line has one element equal to one and all the remaining elements equal to zero. This matrix is defined in the same way as matrix $\mathbf{A}$ (Equation 17).

CONCLUSIONS

Lorem ipsum dolor sit amet, consectetuer adipiscing elit. Ut purus elit, vestibulum ut, placerat ac, adipiscing vitae, felis. Curabitur dictum gravida mauris. Nam arcu libero, nonummy eget, consectetuer id, vulputate a, magna. Donec vehicula augue eu neque. Pellentesque habitant morbi tristique senectus et netus et malesuada fames ac turpis egestas. Mauris ut leo. Cras viverra metus rhoncus sem. Nulla et lectus vestibulum urna fringilla ultrices. Phasellus eu tellus sit amet tortor gravida placerat. Integer sapien est, iaculis in, pretium quis, viverra ac, nunc. Praesent eget sem vel leo ultrices bibendum. Aenean faucibus. Morbi dolor nulla, malesuada eu, pulvinar at, mollis ac, nulla. Curabitur auctor semper nulla. Donec varius orci eget risus. Duis nibh mi, congue eu, accumsan eleifend, sagittis quis, diam. Duis eget orci sit amet orci dignissim rutrum.

Nam dui ligula, fringilla a, euismod sodales, sollicitudin vel, wisi. Morbi auctor lorem non justo. Nam lacus libero, pretium at, lobortis vitae, ultricies et, tellus. Donec aliquet,

tortor sed accumsan bibendum, erat ligula aliquet magna, vitae ornare odio metus a mi. Morbi ac orci et nisl hendrerit mollis. Suspendisse ut massa. Cras nec ante. Pellentesque a nulla. Cum sociis natoque penatibus et magnis dis parturient montes, nascetur ridiculus mus. Aliquam tincidunt urna. Nulla ullamcorper vestibulum turpis. Pellentesque cursus luctus mauris.

Nulla malesuada porttitor diam. Donec felis erat, congue non, volutpat at, tincidunt tristique, libero. Vivamus viverra fermentum felis. Donec nonummy pellentesque ante. Phasellus adipiscing semper elit. Proin fermentum massa ac quam. Sed diam turpis, molestie vitae, placerat a, molestie nec, leo. Maecenas lacinia. Nam ipsum ligula, eleifend at, accumsan nec, suscipit a, ipsum. Morbi blandit ligula feugiat magna. Nunc eleifend consequat lorem. Sed lacinia nulla vitae enim. Pellentesque tincidunt purus vel magna. Integer non enim. Praesent euismod nunc eu purus. Donec bibendum quam in tellus. Nullam cursus pulvinar lectus. Donec et mi. Nam vulputate metus eu enim. Vestibulum pellentesque felis eu massa.

ACKNOWLEDGMENTS

semper nulla. Donec varius orci eget risus. Duis nibh mi, congue eu, accumsan eleifend, sagittis quis, diam. Duis eget orci sit amet orci dignissim rutrum.

REFERENCES

Aster, R. C., B. Borchers, and C. H. Thurber, 2005, Parameter estimation and inverse problems (international geophysics): Academic Press.

Bagherbandi, M., and M. Eshagh, 2012, Crustal thickness recovery using an isostatic model and goce data: Earth, Planets and Space, **64**, 1053–1057.

Barbosa, V. C. F., J. ao B. C. Silva, and W. E. Medeiros, 1997, Gravity inversion of basement relief using approximate equality constraints on depths: Geophysics, **62**, 1745–1757.

Barbosa, V. C. F., J. B. C. Silva, and W. E. Medeiros, 1999a, Gravity inversion of a discontinuous relief stabilized by weighted smoothness constraints on depth: GEOPHYSICS, **64**, 1429–1437.

———, 1999b, Stable inversion of gravity anomalies of sedimentary basins with nonsmooth basement reliefs and arbitrary density contrast variations: GEOPHYSICS, **64**, 754–764.

Barnes, G., and J. Barraud, 2012, Imaging geologic surfaces by inverting gravity gradient data with depth horizons: Geophysics, **77**, G1–G11.

Barzaghi, R., and L. Biagi, 2014, The collocation approach to Moho estimate: Annals of Geophysics.

Bott, M. H. P., 1960, The use of rapid digital computing methods for direct gravity interpretation of sedimentary basins: Geophysical Journal International, **3**, 63–67.

Braitenberg, C., F. Pettenati, and M. Zadro, 1997, Spectral and classical methods in the evaluation of moho undulations from gravity data: The ne italian alps and isostasy: Journal of Geodynamics, **23**, 5 – 22.

Braitenberg, C., and M. Zadro, 1999, Iterative 3d gravity inversion with integration of seismologic data: Bollettino di Geofisica Teorica ed Applicata, **40**, 469–475.

Camacho, A. G., J. Fernndez, and J. Gottsmann, 2011, A new gravity inversion method for

multiple subhorizontal discontinuity interfaces and shallow basins: Journal of Geophysical Research: Solid Earth, **116**.

Chakravarthi, V., and N. Sundararajan, 2007, 3d gravity inversion of basement relief a depth-dependent density approach: GEOPHYSICS, **72**, I23–I32.

Cordell, L., and R. G. Henderson, 1968, Iterative threedimensional solution of gravity anomaly data using a digital computer: GEOPHYSICS, **33**, 596–601.

Dyrelius, D., and A. Vogel, 1972, Improvement of convergency in iterative gravity interpretation: Geophysical Journal of the Royal Astronomical Society, **27**, 195–205.

Gallardo, L. A., M. Péres-Flores, and E. Gómez-Treviño, 2005, Refinement of three-dimensional multilayer models of basins and crustal environments by inversion of gravity and magnetic data: Tectonophysics, **397**, 37 – 54. (Integration of Geophysical and Geological Data and Numerical Models in Basins).

Granser, H., 1987, Three-dimensional interpretation of gravity data from sedimentary basins using an exponential density-depth function: Geophysical Prospecting, **35**, 1030–1041.

Guspí, F., 1993, Noniterative nonlinear gravity inversion: Geophysics, **58**, 935–940.

Hofmann-Wellenhof, B., and H. Moritz, 2005, Physical geodesy: Springer.

Lima, W. A., C. M. Martins, J. B. Silva, and V. C. Barbosa, 2011, Total variation regularization for depth-to-basement estimate: Part 2 physicogeologic meaning and comparisons with previous inversion methods: Geophysics, **76**, I13–I20.

Lowrie, W., 2007, Fundamentals of geophysics: Cambridge University Press. (A second edition of this classic textbook on fundamental principles of geophysics for geoscience undergraduates.).

Martins, C. M., V. C. Barbosa, and J. B. Silva, 2010, Simultaneous 3d depth-to-basement and density-contrast estimates using gravity data and depth control at few points: GEO-

PHYSICS, **75**, I21–I28.

Martins, C. M., W. A. Lima, V. C. Barbosa, and J. B. Silva, 2011, Total variation regularization for depth-to-basement estimate: Part 1 - mathematical details and applications: Geophysics, **76**, I1–I12.

Nagy, D., G. Papp, and J. Benedek, 2000, The gravitational potential and its derivatives for the prism: Journal of Geodesy, **74**, 311–326.

Oldenburg, D. W., 1974, The inversion and interpretation of gravity anomalies: Geophysics, **39**, 526–536.

Pedersen, L. B., 1977, Interpretation of potential field data a generalized inverse approach: Geophysical Prospecting, **25**, 199–230.

Pilkington, M., 2006, Joint inversion of gravity and magnetic data for two-layer models: GEOPHYSICS, **71**, L35–L42.

Pilkington, M., and D. J. Crossley, 1986a, Determination of crustal interface topography from potential fields: GEOPHYSICS, **51**, 1277–1284.

———, 1986b, Inversion of aeromagnetic data for multilayered crustal models: GEOPHYSICS, **51**, 2250–2254.

Reamer, S. K., and J. F. Ferguson, 1989, Regularized twodimensional fourier gravity inversion method with application to the silent canyon caldera, nevada: Geophysics, **54**, 486–496.

Richardson, R. M., and S. C. MacInnes, 1989, The inversion of gravity data into three-dimensional polyhedral models: Journal of Geophysical Research: Solid Earth, **94**, 7555–7562.

Roy, A., 1962, Ambiguity in geophysical interpretation: Geophysics, **27**, 90–99.

Salem, A., C. Green, M. Stewart, and D. D. Lerma, 2014, Inversion of gravity data with

isostatic constraints: GEOPHYSICS, **79**, A45–A50.

Sampietro, D., 2015, Geological units and moho depth determination in the western balkans exploiting goce data: Geophysical Journal International, **202**, 1054–1063.

Shin, Y. H., C.-K. Shum, C. Braitenberg, S. M. Lee, H. Xu, K. S. Choi, J. H. Baek, and J. U. Park, 2009, Three-dimensional fold structure of the tibetan moho from grace gravity data: Geophysical Research Letters, **36**.

Silva, J. B., D. C. Costa, and V. C. Barbosa, 2006, Gravity inversion of basement relief and estimation of density contrast variation with depth: GEOPHYSICS, **71**, J51–J58.

Silva, J. B., A. S. Oliveira, and V. C. Barbosa, 2010, Gravity inversion of 2d basement relief using entropic regularization: Geophysics, **75**, I29–I35.

Silva, J. B. C., and D. F. Santos, 2017, Efficient gravity inversion of basement relief using a versatile modeling algorithm: GEOPHYSICS, **82**, G23–G34.

Silva, J. B. C., D. F. Santos, and K. P. Gomes, 2014, Fast gravity inversion of basement relief: Geophysics, **79**, G79–G91.

Sjöberg, L. E., 2009, Solving vening meinesz-moritz inverse problem in isostasy: Geophysical Journal International, **179**, 1527–1536.

Skeels, D. C., 1947, Ambiguity in gravity interpretation: Geophysics, **12**, 43–56.

Sünkel, H., 1985, An isostatic Earth model: Scientific report 367, Department of Geodetic Science and Surveying, The Ohio State University, Columbus, Ohio.

Tanner, J. G., 1967, An automated method of gravity interpretation: Geophysical Journal of the Royal Astronomical Society, **13**, 339–347.

Turcotte, D. L., and G. Schubert, 2002, Geodynamics, 2. ed. ed.: Cambridge Univ. Press.

Uieda, L., and V. C. Barbosa, 2017, Fast nonlinear gravity inversion in spherical coordinates with application to the south american moho: Geophysical Journal International, **208**,

162–176.

Uieda, L., V. C. Oliveira Jr., and V. C. F. Barbosa, 2013, Modeling the earth with fatiando a terra: Proceedings of the 12th Python in Science Conference, 96 – 103.

van der Meijde, M., J. Julià, and M. Assumpção, 2013, Gravity derived moho for south america: Tectonophysics, **609**, 456 – 467. (Moho: 100 years after Andrija Mohorovicic).

LIST OF FIGURES

1   Rifted margin model formed by four layers. The first one represents a water layer with constant density $\rho^{(w)}$. The second layer is formed by $Q = 2$ vertically adjacent parts. They represent sediments, salt or volcanic rocks and have constant densities $\rho^{(q)}$, $q = 1, \ldots, Q$. The third layer represents the crust, which is divided into the continental crust, with a constant density $\rho^{(cc)}$, and the oceanic crust, with a constant density $\rho^{(oc)}$. We presume an abrupt Crust-Ocean Transition (COT). Finally, the fourth layer of our model represents a homogeneous mantle with constant density $\rho^{(m)}$. Basement and Moho are represented by the dashed-white lines. The continuous white lines represent the isostatic compensation depth at S_0 and the reference Moho at $S_0 + \Delta S$.

2   Interpretation model formed by N columns of vertically stacked prisms. Each column is formed by four layers of prisms and locally approximates the four layers of the rifted margin model (Figure 1). Each prism has a constant density contrast defined as the difference between its corresponding density at the rifted margin model (Figure 1) and the constant density $\rho^{(r)}$ of the shallowest layer forming the reference density distribution (see text). Basement and Moho are represented by the dashed-white lines. The continuous white line represents the isostatic compensation depth at S_0. The base of the interpretation model coincides with the reference Moho located at $S_0 + \Delta S$.
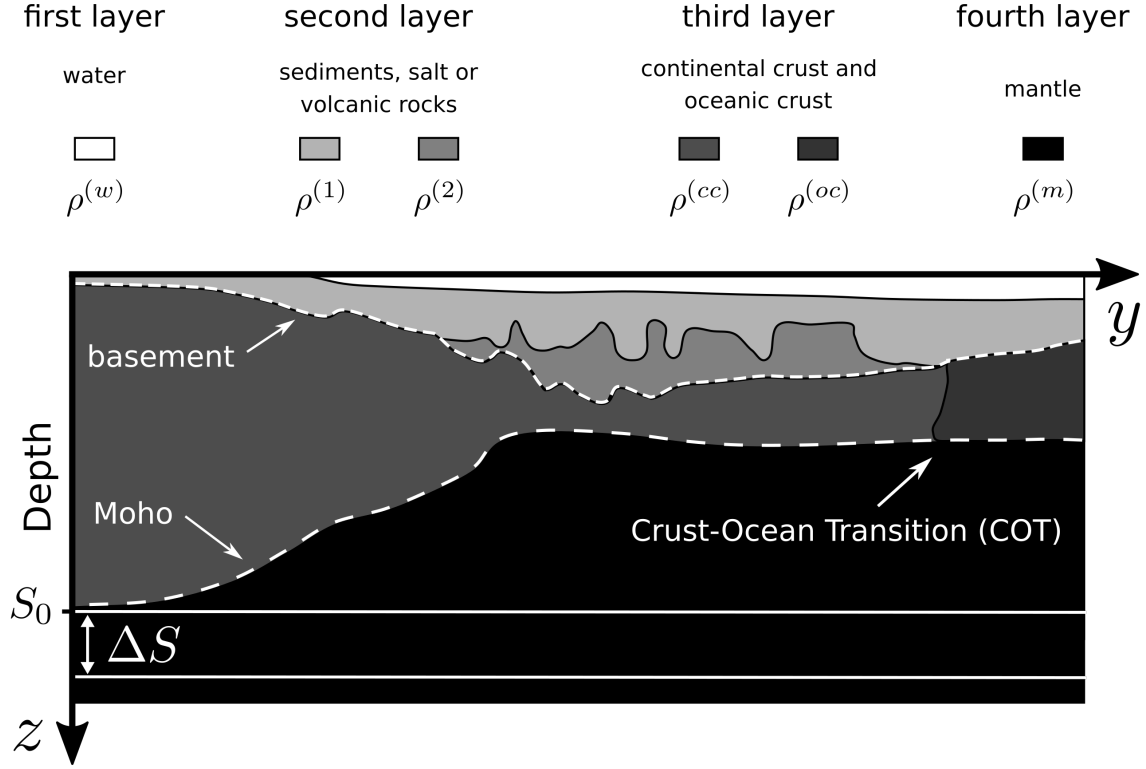
Figure 1: Rifted margin model formed by four layers. The first one represents a water layer with constant density $\rho^{(w)}$. The second layer is formed by $Q = 2$ vertically adjacent parts. They represent sediments, salt or volcanic rocks and have constant densities $\rho^{(q)}$, $q = 1, \ldots, Q$. The third layer represents the crust, which is divided into the continental crust, with a constant density $\rho^{(cc)}$, and the oceanic crust, with a constant density $\rho^{(oc)}$. We presume an abrupt Crust-Ocean Transition (COT). Finally, the fourth layer of our model represents a homogeneous mantle with constant density $\rho^{(m)}$. Basement and Moho are represented by the dashed-white lines. The continuous white lines represent the isostatic compensation depth at S_0 and the reference Moho at $S_0 + \Delta S$.

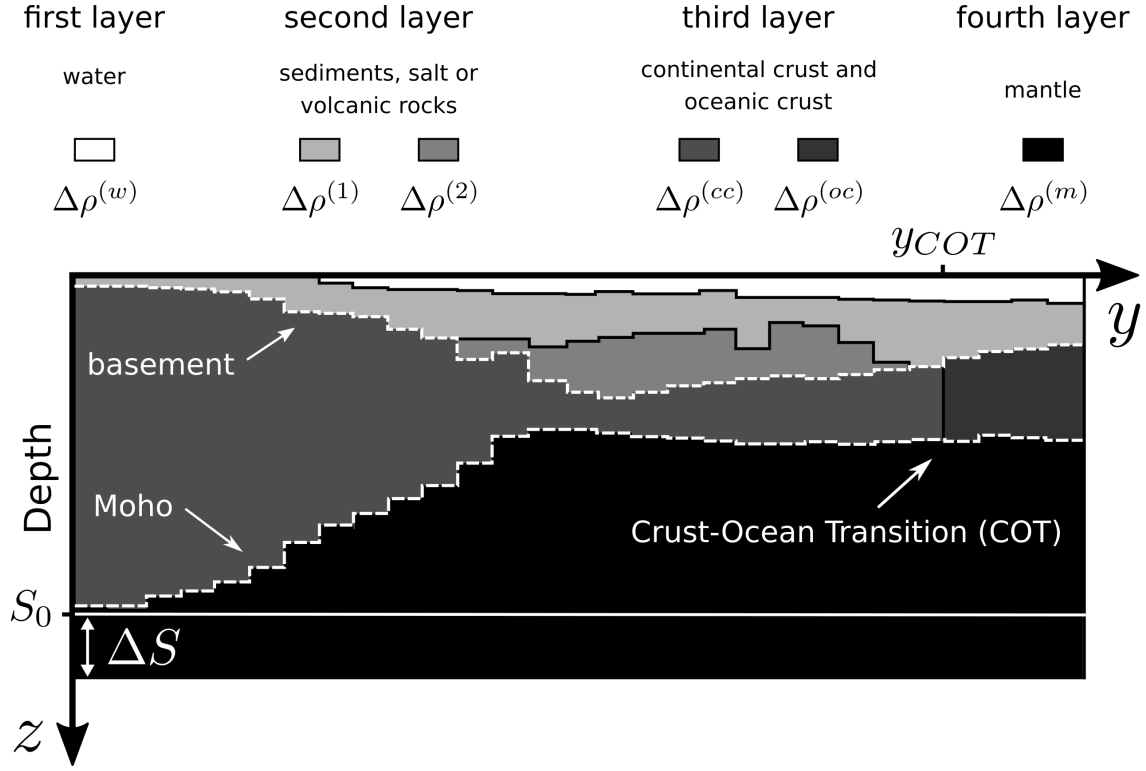**Bastos and Oliveira Jr. – GEO-XXXX**

Figure 2: Interpretation model formed by N columns of vertically stacked prisms. Each column is formed by four layers of prisms and locally approximates the four layers of the rifted margin model (Figure 1). Each prism has a constant density contrast defined as the difference between its corresponding density at the rifted margin model (Figure 1) and the constant density $\rho^{(r)}$ of the shallowest layer forming the reference density distribution (see text). Basement and Moho are represented by the dashed-white lines. The continuous white line represents the isostatic compensation depth at S_0. The base of the interpretation model coincides with the reference Moho located at $S_0 + \Delta S$.

Bastos and Oliveira Jr. – **GEO-XXXX**